Preclinical Evaluation of ^{18}F-PSMA-1007, a New Prostate-Specific Membrane Antigen Ligand for Prostate Cancer Imaging

Jens Cardinale[1], Martin Schäfer[1], Martina Benešová[1], Ulrike Bauder-Wüst[1], Karin Leotta[2], Matthias Eder[1], Oliver C. Neels[1], Uwe Haberkorn[2], Frederik L. Giesel[2], and Klaus Kopka[1]

[1]*Division of Radiopharmaceutical Chemistry, German Cancer Research Center, INF 280, Heidelberg, Germany; and* [2]*Department of Nuclear Medicine, University Hospital Heidelberg, INF 400, Heidelberg, Germany*

In recent years, several radiotracers targeting the prostate-specific membrane antigen (PSMA) have been introduced. Some of them have had a high clinical impact on the treatment of patients with prostate cancer. However, the number of ^{18}F-labeled tracers addressing PSMA is still limited. Therefore, we aimed to develop a radiofluorinated molecule resembling the structure of therapeutic PSMA-617. **Methods:** The nonradioactive reference compound PSMA-1007 and the precursor were produced by solid-phase chemistry. The radioligand ^{18}F-PSMA-1007 was produced by a 2-step procedure with the prosthetic group 6-^{18}F-fluoronicotinic acid 2,3,5,6-tetrafluorophenyl ester. The binding affinity of the ligand for PSMA and its internalization properties were evaluated in vitro with PSMA-positive LNCaP (lymph node carcinoma of the prostate) cells. Further, organ distribution studies were performed with mice bearing LNCaP and PC-3 (prostate cancer cell line; PSMA-negative) tumors. Finally, small-animal PET imaging of an LNCaP tumor–bearing mouse was performed. **Results:** The identified ligand had a binding affinity of 6.7 ± 1.7 nM for PSMA and an exceptionally high internalization ratio (67% ± 13%) in vitro. In organ distribution studies, high and specific tumor uptake (8.0 ± 2.4 percentage injected dose per gram) in LNCaP tumor–bearing mice was observed. In the small-animal PET experiments, LNCaP tumors were clearly visualized. **Conclusion:** The radiofluorinated PSMA ligand showed promising characteristics in its preclinical evaluation, and the feasibility of prostate cancer imaging was demonstrated by small-animal PET studies. Therefore, we recommend clinical transfer of the radioligand ^{18}F-PSMA-1007 for use as a diagnostic PET tracer in prestaging and monitoring of prostate cancer.

Key Words: PSMA; ^{18}F; prostate cancer; PET

J Nucl Med 2017; 58:425–431
DOI: 10.2967/jnumed.116.181768

The prostate-specific membrane antigen (PSMA) is strongly overexpressed in most prostate cancers and offers a versatile target for imaging and therapy (*1*). Therefore, several PSMA-targeting tracers have been developed during the last 2 decades (*2*). Some of the most clinically potent compounds are listed in Table 1.

Two major contributions to the field are represented by the urea-based peptidomimetic substances PSMA-11 (*3*) and PSMA-617 (*4*) (Fig. 1). Although both compounds can be labeled with the short-lived radioisotope ^{68}Ga, the latter offers broader opportunities for labeling with a DOTA chelator including ^{177}Lu and ^{225}Ac.

^{68}Ga-labeled PSMA-11 was introduced in 2012 (*3*) and, after its clinical application (*5*), quickly evolved to being the most commonly used radiotracer for PSMA PET imaging of prostate cancer (*1*). The radionuclide ^{68}Ga is introduced to PSMA-11 via the chelator *N*,*N*′-*bis*[2-hydroxy-5-(ethylene-β-carboxy)benzyl]ethylenediamine-*N*,*N*′-diacetic acid (HBED-CC). However, the chelating agent HBED-CC cannot form stable complexes with the trivalent therapeutic radionuclides ^{177}Lu, ^{90}Y, and ^{225}Ac. Hence, a compound bearing a DOTA chelator while maintaining the binding properties of PSMA-11 was of clinical interest.

As a consequence, PSMA-617 was designed and introduced in 2015 (*4*). The structural key element of PSMA-617 is its linker design, which triggers binding and internalization of the substance through a presumed interaction of the rigid (tranexamic acid) and aromatic (2-naphthylalanine) amino acids with rigid parts of the PSMA binding pocket (*6*). Although prospective clinical trials are still pending, the ^{177}Lu- and ^{225}Ac-labeled versions of this PSMA inhibitor have already proved its therapeutic potential (*7–14*).

Both ^{68}Ga-PSMA-11 and PSMA-617 (^{177}Lu or ^{225}Ac labeled) principally cover the diagnostic and therapeutic aspects of clinical prostate cancer care. However, a major drawback of ^{68}Ga is related to the availability of the radionuclide; at present, commercially available ^{68}Ge/^{68}Ga generators can offer a maximum activity of 1.85 GBq of ^{68}Ga (88.9% β^+; half-life, 67.71 min). This limitation confines the average batch production of the desired tracer to approximately 2–4 patient doses, depending on the usage of the radionuclide generator. An alternative is the cyclotron production of ^{68}Ga with a liquid target (*15*), but this method so far has not been established as a standard for large-scale production and thus cannot guarantee reliable provision of the tracer. Together with the short half-life of ^{68}Ga, this limitation results in the necessity of several rounds of production per day for sustaining the clinical routine. Hence, there is a strong demand for ^{18}F-labeled PSMA-targeting radiotracers (96.7% β^+; half-life, 109.77 min).

In principle, such a compound is already available in the form of 2-(3-(1-carboxy-5-[(6-^{18}F-fluoro-pyridine-3-carbonyl)-amino]-pentyl)-ureido)-pentanedioic acid (*16*). However, we aimed to develop a radiofluorinated tracer mimicking the biodistribution

Received Aug. 4, 2016; revision accepted Sep. 27, 2016.
For correspondence or reprints contact: Jens Cardinale, DKFZ, INF 280, 69120 Heidelberg, Germany.
E-mail: j.cardinale@dkfz.de
Published online Oct. 27, 2016.

TABLE 1
Clinically Relevant PSMA-Targeting Molecules

Compound	Class	Label	Reference
MIP-1095	Therapeutic	^{124}I, ^{131}I	*22,23*
MIP-1404	Diagnostic	^{99m}Tc	*24*
DCFBC	Diagnostic	^{18}F	*25*
DCFPyL	Diagnostic	^{18}F	*26*
PSMA I&T	Theranostic	^{68}Ga, ^{177}Lu	*27*
PSMA-11	Diagnostic	^{68}Ga	*3*
PSMA-617	Theranostic	^{68}Ga, ^{90}Y, ^{177}Lu, ^{225}Ac	*4*

behavior of labeled PSMA-617, thereby making use of its adjusted linker design. Because of the need for alternative ^{18}F-labeled PSMA tracers and to complete a theranostic in tandem with ^{177}Lu-PSMA-617, we report here the preclinical characterization of our leading candidate, ^{18}F-PSMA-1007, which we recommend for first-in-human studies in patients with prostate cancer (*17*).

MATERIALS AND METHODS

All chemicals, reagents, and solvents used were at least synthesis grade; were purchased from Sigma Aldrich, VWR, Iris Biotech, and Carl Roth; and were used without further purification.

When means are given, the respective errors are reported as SDs. For in vitro experiments, each result from a single experiment was determined in triplicate or quadruplicate within the experiment, and the experiments were repeated multiple times. The errors of the means were then calculated as SDs; the errors for the results of single experiments were ignored.

The patient scan shown in Figure 2 was taken from a first-in-human study that was ethically approved by the Institutional Review Board of the University Hospital Heidelberg in accordance with national regulations in Germany and the updated version of the Helsinki Declaration (permit S321/2012).

Synthesis of Precursor Molecules and Reference Compound

The synthesis of *N*,*N*,*N*-trimethyl-5-((2,3,5,6-tetrafluorophenoxy)-carbonyl)pyridine-2-aminium trifluoromethansulfonate as a precursor for the radiosynthesis of the prosthetic group 6-^{18}F-fluoronicotinic acid 2,3,5,6-tetrafluorophenyl ester (6-^{18}F-F-Py-TFP) was accomplished as described by Olberg et al. (*18*).

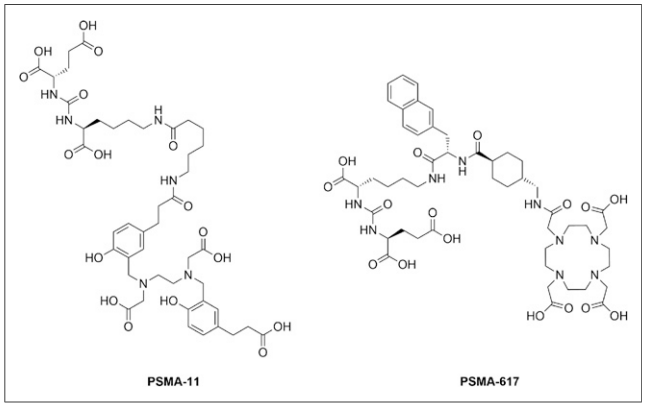

FIGURE 1. Chemical structures of PSMA-11 and PSMA-617 (lead structure).

The synthesis of the precursor for ^{18}F-PSMA-1007 (compound 1) as well as the reference compound PSMA-1007 (compound 2) was accomplished by well-established methods and is summarized in Figure 3. In brief, the binding motif consisting of the amino acids glutamine and lysine, linked via their α-amino groups by a carbonyl forming a urea group, was built upon a solid phase from resin-bound allyloxycarbonyl-protected lysine 3 and the isocyanate of *bis-tert*-butyl–protected glutamic acid 4 (*3*). Subsequently, the linker was produced by standard fluorenylmethoxycarbonyl solid-phase synthesis (*3,4,6*). Then, the precursor (compound 1) was prepared by cleavage from the resin and deprotection, and the nonradioactive reference compound (compound 2) was prepared via the intermediate compound (compound 7) and subsequent cleavage and deprotection.

Radiosynthesis of ^{18}F-PSMA-1007

Preparation and Activation of No-Carrier-Added ^{18}F-Fluoride. ^{18}F was produced by irradiation of ^{18}O-enriched water (Rotem Industries Ltd.) with 16.5-MeV proton beams in the ^{18}O(p,n)^{18}F nuclear reaction. Irradiation was performed with the Scanditronix MC32NI cyclotron at the Division of Radiopharmaceutical Chemistry, German Cancer Research Center, Heidelberg, Germany.

After transfer of the irradiated water to an automated radiosynthesizer system (Trasis AllInOne), ^{18}F-F$^-$ was separated from irradiated ^{18}O-H_2O by passage through a preconditioned (5 mL of 1 M K_2CO_3 and 10 mL of water) anion-exchange cartridge (Waters Accel Plus QMA Cartridge Light) and elution with a mixture of 800 μL of acetonitrile and 150 μL of tetrabutylammonium bicarbonate solution (320 mM in ultrapure water). The mixture was then evaporated to dryness at a temperature of 100°C under a stream of nitrogen. This azeotropic drying was repeated 2 times by adding 1.8 mL of acetonitrile for each step. After application of the maximum achievable vacuum to the reaction vessel for 90 s at 80°C and subsequent cooling to 50°C, the dry residue was dissolved in 2 mL of *tert*-butanol–acetonitrile (8:2, v/v); this solution was used for the radiolabeling reactions.

Preparation of No-Carrier-Added 6-^{18}F-F-Py-TFP. The preparation of the prosthetic group 6-^{18}F-F-Py-TFP was accomplished with a slight modification of the previously reported procedure (*18*). After trapping of 6-^{18}F-F-Py-TFP on an Oasis MCX Plus Sep-Pak cartridge (Waters) and subsequent washing steps, the cartridge was rinsed with the eluent (acetonitrile–water, 65:35, v/v) in fractions of 400 and 500 μL. Although a negligible amount of radioactivity was contained in the first

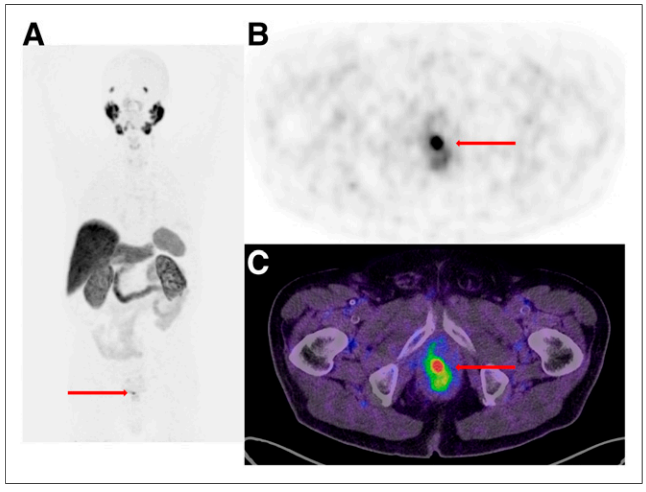

FIGURE 2. PET/CT of patient with prostate cancer 1 h after injection of ^{18}F-PSMA-1007. Arrows indicate lesions. (A) Maximum-intensity projection. (B) Axial view of pelvic region. (C) Fusion of PET scan and CT scan (pelvic region; axial view).

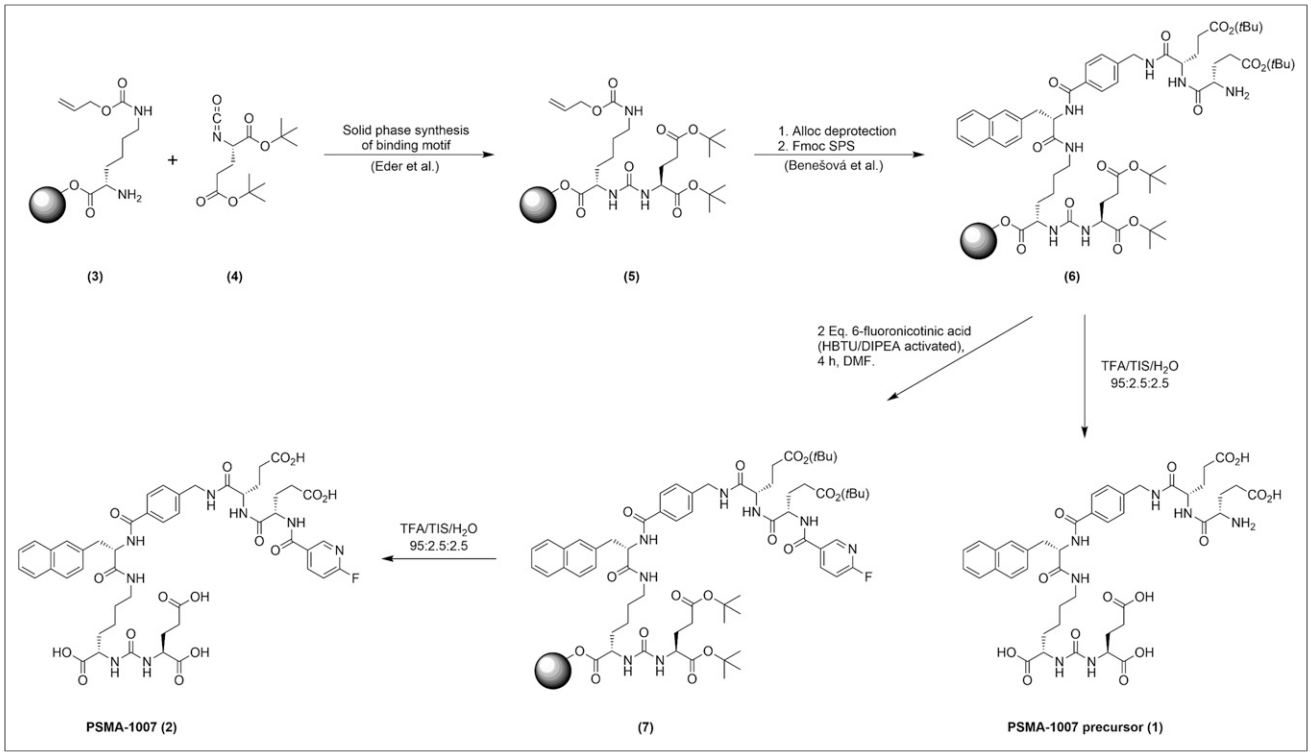

FIGURE 3. Synthesis of precursor (compound 1) and PSMA-1007 (compound 2) (*3,4,6*). Alloc = allyloxy-carbonyl; DIPEA = *N,N*-diisopropylethylamine; DMF = *N,N*-dimethylformamide; Fmoc = fluorenylmethoxycarbonyl; HBTU = 2-(1H-benzotriazol-1-yl)-1,1,3,3-tetramethyluronium hexafluorophosphate; SPS = solid-phase synthesis; TFA = trifluoroacetic acid; TIS = triisopropylsilane.

fraction, usually more than 50% of the product activity was contained in the second fraction (typically 1.0–2.0 GBq); the latter was used for the radiolabeling reactions.

^{18}F-PSMA-1007. A 400-μL quantity of 6-^{18}F-F-Py-TFP solution was mixed with 100 μL of a solution of compound 1 (2 mg/mL in dimethyl sulfoxide; 220 nmol) in the presence of 100 μL of phosphate buffer (0.2 M; pH 9.0), and the mixture was heated at 60°C for 20 min. The product was separated from the crude mixture by semipreparative high-performance liquid chromatography (HPLC) with a Merck Chromolith Performance RP-18e column (100–10 mm), a multistep gradient of solvent A (acetonitrile) and solvent B (water–0.1% trifluoroacetic acid) (100% B → 65% B [2 min] → 50% B [6 min] → 5% B [8 min] → 5% B [10 min]; with A + B = 100%), a flow rate of 4 mL/min, and a retention time of 4.37 min; the product was collected from 4.3 to 4.6 min. Subsequently, the product was concentrated on a Sep-Pak C18 cartridge (Waters) and eluted in 1 mL of ethanol–water (70:30, v/v).

Formulation. For formulation, the amount of carrier was adjusted appropriately to the respective assays with radiometal-labeled PSMA ligands (where the carrier was the nonseparated precursor peptide). The ethanol–water mixture containing ^{18}F-PSMA-1007 was dried at 98°C under a stream of nitrogen, and then the product was dissolved either in a 6 μM solution of the nonradioactive reference compound (compound 2) in 0.9% NaCl for in vitro experiments (~100 MBq/mL) or in a 0.6 μM solution of compound 2 in 0.9% NaCl for organ distribution studies (~10–20 MBq/mL). For the small-animal PET experiments, the product was dissolved in 0.9% NaCl, the specific activity was determined by HPLC, and the solution was diluted to a final concentration of 0.6 μmol/L.

In Vitro Experiments

Cell Culture. For binding studies and in vivo experiments, LNCaP (lymph node carcinoma of the prostate; CRL-1740; American Type Culture Collection) cells were cultured in RPMI 1640 (PAN Biotech) medium supplemented with 10% fetal calf serum and stable glutamine (PAN Biotech). Cells were grown at 37°C in an incubator with humidified air equilibrated with 5% CO_2.

Cell Binding and Internalization. The competitive cell binding assays and internalization experiments were performed as described previously (*6*). In brief, LNCaP cells (10^5/well) were incubated with a ^{68}Ga-labeled radioligand—[Glu-urea-Lys(Ahx)]$_2$-[^{68}Ga(HBED-CC)] (^{68}Ga-PSMA-10) (*19*)—at a concentration of 0.75 nM in the presence of 12 different concentrations of compound 2 (0–5,000 nM; 100 μL/well). After incubation, washing was performed with a multiscreen vacuum manifold (Millipore). Cell-bound radioactivity was measured with a γ-counter (Packard Cobra II; GMI). The 50% inhibitory concentrations were calculated by fitting the data with a nonlinear regression algorithm (GraphPad Prism 5.01 software). Experiments were performed in quadruplicate.

For the determination of specific cellular uptake and internalization, 10^5 cells were seeded in poly-L-lysine–coated 24-well cell culture plates for 24 h. The cells in each well were incubated with 250 μL of a 30 nM solution of carrier-added ^{18}F-PSMA-1007 (15–20 GBq/μmol) in Opti-MEM I medium (Gibco). Specific cellular uptake was determined by blocking with 2-(phosphonomethyl)pentanedioic acid (2-PMPA) (final concentration, 500 μM; Axxora). All experiments were conducted at 37°C and 4°C. The incubation was terminated after 45 min by washing 3 times with 1 mL of ice-cold phosphate-buffered saline. The cells were subsequently incubated twice with 0.5 mL of glycine HCl (50 mM; pH 2.8) for 5 min each to remove the surface-bound fraction, and the supernatant was collected. After an additional washing step with 1 mL of ice-cold phosphate-buffered saline, the cells were lysed with 0.5 mL of NaOH (0.3N) and collected, and radioactivity was measured with a γ-counter. Specific cellular uptake was calculated as a percentage of

TABLE 2
Summary of Analytic Results for Compounds 1 and 2

Compound	*m/z* calculated	*m/z* found	HPLC retention time (min)	Purity determined by HPLC at: 254 nm	220 nm
1	908.93	908.7	3.74	>97.3%	>97.3%
2	1,032.01	1,032.1	4.49	>96.5%	>98.1%

HPLC was performed with Merck Chromolith Performance RP-18e column (100–4.6 mm), gradient of 5% solvent A (acetonitrile)/95% solvent B (0.1% aqueous trifluoroacetic acid) to 95% A/5% B in 12.5 min, flow of 3 mL/min, and dead time of 0.56 min.

the initially added radioactivity bound to 10^5 cells (%IA/10^5 cells) by subtraction of the respective uptake under blocking conditions. All experiments were conducted in triplicate.

Plasma Stability. For the determination of plasma stability, 400 μL of human plasma AB (Sigma-Aldrich) were incubated with 40 μL of the 6 μM carrier-added ^{18}F-PSMA-1007 formulation (100 MBq/mL) at 37°C. After 1, 2, and 4 h, samples of 100 μL were removed from the mixture, the protein was precipitated by the addition of 100 μL of acetonitrile and separated from the liquid by centrifugation at 13,000 rpm (2 times), and the liquid was analyzed by HPLC.

In Vivo and Organ Distribution Experiments

All animal experiments were conducted in compliance with the current laws of the Federal Republic of Germany. For in vivo and organ distribution experiments, 8-wk-old male BALB/c *nu/nu* mice were subcutaneously inoculated in the right trunk with 6×10^6 LNCaP cells in 50% Matrigel (Corning) or 5×10^6 PC-3 (prostate cancer cell line; PSMA-negative) cells in Opti-MEM I medium. The organ distribution studies were performed when the size of the tumor was approximately 1 cm^3.

Organ Distribution. Organ distribution studies were performed with mice bearing an LNCaP tumor with or without 2-PMPA blockade and mice bearing a PC-3 tumor. Each experiment was conducted in triplicate. For the blockade experiment, the mice were administered 0.4 mM 2-PMPA (100 μL; 40 nmol) via tail vein injection 30 min before injection of the tracer. PSMA-1007 was administered as a 0.6 μM solution (100 μL; 60 pmol) spiked with 1–2 MBq of ^{18}F-PSMA-1007 via tail vein injection. At 1 h after injection, the animals were sacrificed (CO_2 asphyxiation), and organs of interest were dissected, blotted dry, and weighed. Radioactivity was measured with a γ-counter (Packard Cobra II) and calculated as the percentage injected dose per gram (%ID/g).

Dynamic PET Experiments. For the small-animal PET experiments, 100 μL of 0.6 μM carrier-added ^{18}F-PSMA-1007 (~420 GBq/μmol; 60 pmol; 25 MBq) were injected via a lateral tail vein into a mouse bearing an LNCaP tumor xenograft. The anesthetized animal (2% sevoflurane; Abbott) was placed in the prone position in an Inveon small-animal PET scanner (Siemens) for a dynamic small-animal PET scan. Before the scan, the transmission was measured for 900 s with a rotating ^{57}Co source. Acquisition was started 3 s before the tracer was injected and was continued for 3,600 s in the list mode. The radial field of view was 7.5 cm. A second scan was performed 2 h after injection. Between the first scan and the second scan, the mouse was allowed to wake up.

The scans were reconstructed by use of Acquisition Workplace software (Siemens) with a 28-frame protocol (2×15 s, 8×30 s, 5×60 s, 5×120 s, and 8×300 s). The volumes of interest for the generation of the time–activity curves were drawn manually over the respective organs. Reconstruction of the images was done with an ordered-subset expectation maximization 3-dimensional maximum a posteriori algorithm (maximum a posteriori iterations, 18; output interval, 20; image *x–y* size, 256; image *z* size, 161; size of voxel, 0.43 mm for *x–y* and 0.796 mm for *z*).

RESULTS

Synthesis of Precursor Molecules and Reference Compound

The results of the synthesis of the precursor and the reference compound are summarized in Table 2. A production batch usually resulted in 20–50 mg of the desired product, equivalent to a yield of 13%–30%.

Radiosynthesis of ^{18}F-PSMA-1007

The initial labeling reaction delivered the prosthetic group 6-^{18}F-F-Py-TFP in non–decay-corrected yields of 30%–60% after a synthesis time of 10–15 min (including cartridge separation). The final coupling delivered the labeled product ^{18}F-PSMA-1007 in yields of 5%–10% after an additional synthesis time of 30 min (including HPLC separation). Therefore, the non–decay-corrected yield was 1.5%–6.0% overall (typically 40–160 MBq in 600 μL of reaction solvent) after a total synthesis time of approximately 45 min (without the fluoride drying and formulation steps).

In Vitro Experiments

Competitive cell binding experiments with LNCaP cells and ^{68}Ga-PSMA-10 revealed a nanomolar inhibition potency toward PSMA (inhibition constant, 6.7 ± 1.7 nM; $n = 3$). Moreover, the surface-bound and internalized fractions of ^{18}F-PSMA-1007 on LNCaP cells, determined ($n = 10$) with 2.14 ± 0.64 and 5.01 ± 2.70 %IA/10^5 cells, respectively, led to a total internalization ratio of 67% ± 13% (internalized/total bound activity). The respective values determined for ^{177}Lu-PSMA-617 by the same procedures—an inhibition constant of 2.3 ± 2.9 nM, 1.1 ± 0.7 %IA/10^5 cells surface bound, and 1.6 ± 0.4 %IA/10^5 cells internalized—led to a total internalization ratio of 58% (*6*). In the plasma stability test, we did not observe any decomposition after 4 h (radiochemical purity, >99%) by HPLC.

In Vivo and Organ Distribution Experiments

The results of the organ distribution experiments are summarized in Table 3, and the results of the small-animal PET experiments are shown in Figures 4 and 5. The SUV_{mean} body weight values between 120 and 140 min after injection—0.23 (heart), 0.20 (liver), 7.6 (kidneys), 27.2 (bladder), 0.13 (muscle), 0.16 (bone),

TABLE 3
Results of Organ Distribution Experiments at 1 Hour After Injection

Organ	Uptake (%ID/g) in:		
	LNCaP tumor, no blockade	LNCaP tumor, 2-PMPA blockade	PC-3 tumor, PSMA-negative
Blood	0.60 ± 0.21	0.41 ± 0.13	0.77 ± 0.29
Heart	1.11 ± 0.20	0.41 ± 0.07	1.45 ± 0.10
Lung	1.25 ± 0.27	0.78 ± 0.04	2.09 ± 0.33
Spleen	6.99 ± 1.04	1.40 ± 0.27	12.44 ± 5.98
Liver	1.06 ± 0.20	0.43 ± 0.03	1.14 ± 0.16
Kidney	84.03 ± 13.85	9.72 ± 2.50	142.08 ± 25.82
Muscle	0.79 ± 0.28	0.40 ± 0.19	0.94 ± 0.47
Small intestine	0.90 ± 0.21	0.46 ± 0.10	1.20 ± 0.18
Brain	0.12 ± 0.04	0.07 ± 0.03	0.10 ± 0.01
Tumor	8.04 ± 2.39	4.26 ± 2.06	1.05 ± 0.11

All mice were injected with 1–2 MBq of ^{18}F-PSMA-1007 (carrier added; 60 pmol/injection). Mice bore either PSMA-positive LNCaP or PSMA-negative PC-3 tumors. In blockade experiment, tracer was injected 30 min after administration of 40 nmol of 2-PMPA (n = 3 mice per column). Data are mean ± SD.

and 1.6 (tumor)—resulted in a tumor-to-muscle ratio of 12.3 and a tumor-to-blood ratio of 7.0.

The time–activity curves (Fig. 4) showed fast uptake in the tumor and rapid clearance from nontarget organs, except for the kidneys. The tracer showed some uptake in bone that declined over time, so that defluorination of the tracer could be excluded. Directly after administration, the tumor-to-muscle and tumor-to-blood ratios started to increase constantly over time (Fig. 4). This result was also reflected in the maximum-intensity projections shown in Figure 5. The tumor became visible between 20 and 40 min after injection and showed constantly improving contrast over the following hour.

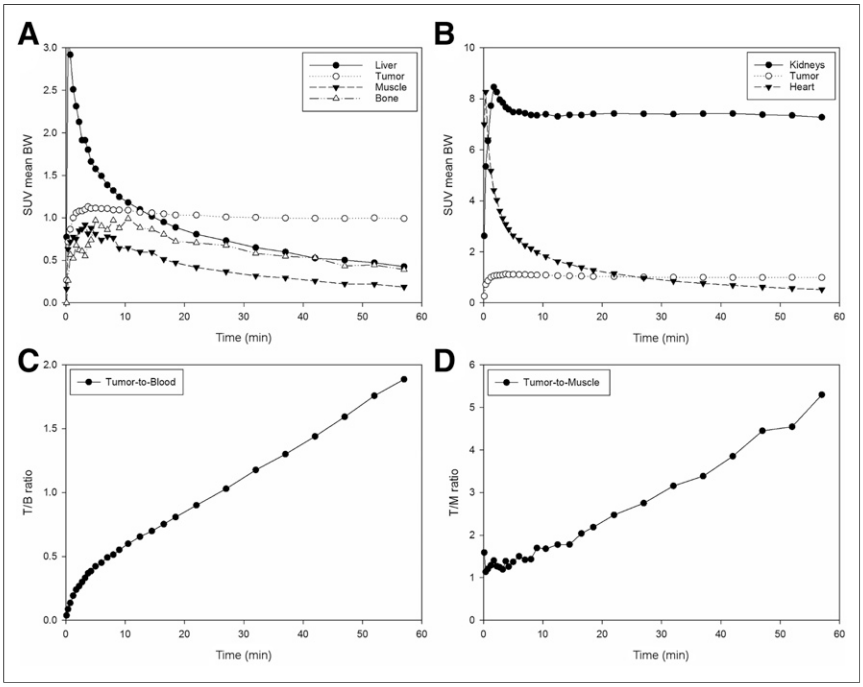

FIGURE 4. (A and B) Time–activity curves from small-animal PET experiment with BALB/c *nu/nu* mouse bearing LNCaP tumor after injection of 25 MBq of carrier-added ^{18}F-PSMA-1007. BW = body weight. (C and D) Corresponding tumor-to-blood (T/B) (calculated from SUV_{mean} for heart) (C) and tumor-to-muscle (T/M) (D) ratios.

DISCUSSION

The main goal of the present study was the identification of an ^{18}F-labeled PSMA ligand based on the structure of PSMA-617 to complete a theranostic in tandem with ^{177}Lu-PSMA-617. In an extensive preclinical study that will be reported elsewhere, ^{18}F-PSMA-1007 was identified as a leading candidate for that purpose. Here we report the preclinical characterization of ^{18}F-PSMA-1007.

Synthesis of Precursor Molecules and Reference Compound

The preparation of the precursor (compound 1) and the nonradioactive reference compound PSMA-1007 (compound 2) could be accomplished easily with previously described methods. The process delivered material in sufficient amounts and of adequate purity for preclinical investigations.

Radiosynthesis of ^{18}F-PSMA-1007

The preparation of the secondary precursor 6-^{18}F-F-Py-TFP was reproducible and proved to be convenient because of its separation by cartridge extraction. However, conjugation of this prosthetic group to the peptidomimetic precursor (compound 1) delivered the desired product, ^{18}F-PSMA-1007, only in low yields (5%–10%). This result could be explained by presumed inner salt

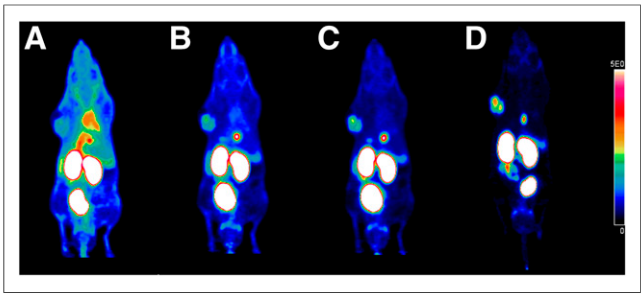

FIGURE 5. Whole-body coronal small-animal PET scans as maximum-intensity projections of BALB/c *nu/nu* mouse bearing LNCaP tumor 0–20 (A), 20–40 (B), 40–60 (C), and 120–140 (D) min after injection of 25 MBq of ^{18}F-PSMA-1007 (~60 pmol).

formation in the terminal glutamic acid, which could lead to reduced reactivity of the amino group with the 2,3,5,6-tetrafluorophenyl ester. Only small amounts of radioactivity were required for the preclinical experiments, and the purity of the product was sufficient.

In Vitro Experiments

The urea-based peptidomimetic compound (compound 2) showed a nanomolar binding affinity for PSMA. Moreover, we confirmed high and specific uptake of ^{18}F-PSMA-1007 in PSMA-positive LNCaP cells. This result was expected because of the marked similarity of compound 2 to the lead structure which, in turn, was the leading candidate selected from a library of PSMA ligands for the imaging and therapy of prostate cancer (*6*). Surprisingly, a high internalization ratio (67%) was observed in our in vitro experiments (for comparison, the respective value for PSMA-617 is 58%) (*6*).

In Vivo and Organ Distribution Experiments

In organ distribution experiments, the radiotracer showed high tumor uptake (8.0 ± 2.4 %ID/g) 1 h after administration. The uptake in nontarget tissue was rather low, except for the spleen and kidneys. However, this result was expected, at least for the kidneys, because PSMA is also expressed there (*20*). This result was also reflected in the findings from the blockade experiment, as a significant reduction in uptake in both organs was observed, indicating that uptake in the spleen was also specific.

Further organ distribution experiments were conducted to prove the specificity of tumor uptake. The blockade experiment with 2-PMPA as a competing ligand led to a significant, but not complete, reduction in tumor uptake. This result might be attributable to the binding mechanism of 2-PMPA, as it has been reported to be a fast and reversible inhibitor (*21*). Given the high internalization ratio of ^{18}F-PSMA-1007, only a small fraction of the ligand needs to be bound to be internalized—even in the presence of the competitor—and thus might result in significant uptake into the tumor. A larger amount of blocking substance might reduce the uptake of ^{18}F-PSMA-1007 further. An additional organ distribution experiment with PSMA-negative PC-3 tumor–bearing mice revealed low tumor uptake (~1.1 ± 0.1 %ID/g). In summary, the uptake of ^{18}F-PSMA-1007 could be blocked by a sufficient amount of 2-PMPA, indicating the high specificity of the tracer.

Finally, the feasibility of prostate cancer imaging with ^{18}F-PSMA-1007 was demonstrated in a dynamic PET experiment with a mouse bearing an LNCaP tumor. The tracer showed the typical uptake in the kidneys and clearance via the renal pathway. However, the tumor was clearly visualized 40 min after injection, and uptake in all nontarget organs, except the kidneys, declined over time—leading to constantly improving tumor-to-background ratios. Therefore, we clearly demonstrated the feasibility of PET imaging of prostate cancer with ^{18}F-PSMA-1007 as a new radiotracer.

Outlook

At present, a first-in-human study is being conducted with ^{18}F-PSMA-1007. Therefore, a good manufacturing practices–compliant (2-step) method for synthesis of the tracer has been developed and will be reported elsewhere. One of the first PET images acquired in that study is shown in Figure 2. A 76-y-old patient with an elevated prostate-specific antigen level was referred for nuclear medicine to undergo PSMA PET/CT before surgery. PSMA PET detected intraprostatic PSMA accumulation in the peripheral apical zone on the right without any suggestion of tumor spread outside the prostate gland. This result clearly underlined successful translation to a clinical setting.

CONCLUSION

At present, ^{18}F-labeled PSMA ligands are needed for the clinical diagnosis of prostate cancer by means of PET/CT and PET/MRI. As part of an extended preclinical study, the compound ^{18}F-PSMA-1007 was identified as a leading diagnostic candidate for noninvasive PET imaging of prostate cancer. ^{18}F-PSMA-1007 might also be useful for planning PSMA ligand therapy with its therapeutic counterpart, PSMA-617. The ligand showed promising binding and internalization properties in vitro as well as high and specific uptake in vivo. The feasibility of prostate cancer imaging with ^{18}F-PSMA-1007 was further demonstrated by a dynamic small-animal PET experiment.

DISCLOSURE

This project was supported by a postdoctoral scholarship from ABX Advanced Biochemical Compounds GmbH (DKFZ file no. L-15309). ^{18}F-PSMA-1007 is the subject of a patent application by Jens Cardinale, Martin Schäfer, Martina Benešová, Ulrike Bauder-Wüst, Matthias Eder, Uwe Haberkorn, Frederik Giesel, and Klaus Kopka. No other potential conflict of interest relevant to this article was reported.

ACKNOWLEDGMENTS

We thank Yvonne Remde for support in establishing the radiosynthesis of ^{18}F-PSMA-1007 and Oksana Hautzinger and Uschi Schierbaum for support with the organ distribution and small-animal PET experiments.

REFERENCES

1. Rowe SP, Gorin MA, Allaf ME, et al. PET imaging of prostate-specific membrane antigen in prostate cancer: current state of the art and future challanges. *Prostate Cancer Prostatic Dis.* 2016;19:223–230.
2. Kiess AP, Banerjee SR, Mease RC, et al. Prostate-specific membrane antigen as a target for cancer imaging and therapy. *Q J Nucl Med Mol Imaging.* 2015;59:241–268.
3. Eder M, Schäfer M, Bauder-Wüst U, et al. ^{68}Ga-complex lipophilicity and the targeting property of a urea-based PSMA inhibitor for PET imaging. *Bioconjug Chem.* 2012;23:688–697.
4. Benešová M, Schäfer M, Bauder-Wüst U, et al. Preclinical evaluation of a tailor-made DOTA-conjugated PSMA inhibitor with optimized linker moiety for imaging and endoradiotherapy of prostate cancer. *J Nucl Med.* 2015;56:914–920.

5. Afshar-Oromieh A, Haberkorn U, Eder M, Eisenhut M, Zechmann CM. [^{68}Ga] gallium-labelled PSMA ligand as superior PET tracer for the diagnosis of prostate cancer: comparison with ^{18}F-FECH. *Eur J Nucl Med Mol Imaging.* 2012;39:1085–1086.
6. Benešová M, Bauder-Wüst U, Schäfer M, et al. Linker modification strategies to control the prostate-specific membrane antigen (PSMA)-targeting and pharmacokinetic properties of DOTA-conjugated PSMA inhibitors. *J Med Chem.* 2016; 59:1761–1775.
7. Kratochwil C, Giesel FL, Stefanova M, et al. PSMA-targeted radionuclide therapy of metastatic castration-resistant prostate cancer with ^{177}Lu-labeled PSMA-617. *J Nucl Med.* 2016;57:1170–1176.
8. Delker A, Fendler WP, Kratochwil C, et al. Dosimetry for ^{177}Lu-DKFZ-PSMA-617: a new radiopharmaceutical for the treatment of metastatic prostate cancer. *Eur J Nucl Med Mol Imaging.* 2016;43:42–51.
9. Rahbar K, Schmidt M, Heinzel A, et al. Response and tolerability of single dose of ^{177}Lu-PSMA-DKFZ-617 in patients with metastatic castration-resistant prostate cancer: a multicenter retrospective analysis. *J Nucl Med.* 2016;57:1334–1338.
10. Das T, Guleria M, Parab A, et al. Clinical translation of ^{177}Lu-labeled PSMA-617: initial experience in prostate cancer patients. *Nucl Med Biol.* 2016;43:296–302.
11. Kabasakal L, AbuQbeitah M, Aygün A, et al. Pre-therapeutic dosimetry of normal organs and tissues of ^{177}Lu-PSMA-617 prostate-specific membrane antigen (PSMA) inhibitor in patients with castration-resistant prostate cancer. *Eur J Nucl Med Mol Imaging.* 2015;42:1976–1983.
12. Schlenkhoff CD, Gaertner F, Essler M, Schmidt M, Ahmadzadehfar H. Positive influence of ^{177}Lu PSMA-617 therapy on bone marrow depression caused by metastatic prostate cancer. *Clin Nucl Med.* 2016;41:478–480.
13. Hohberg M, Eschner W, Schmidt M, et al. Lacrimal glands may represent organs at risk for radionuclide therapy of prostate cancer with [^{177}Lu]DKFZ-PSMA-617. *Mol Imaging Biol.* 2016;18:437–445.
14. Kratochwil C, Bruchertseifer F, Giesel FL, et al. ^{225}Ac-PSMA-617 for PSMA targeting alpha-radiation therapy of patients with metastatic castration-resistant prostate cancer. *J Nucl Med.* July 7, 2016 [Epub ahead of print].
15. Pandey MK, Byrne JF, Jiang H, Packard AB, DeGrado TR. Cyclotron production of ^{68}Ga via the ^{68}Zn(p,n)^{68}Ga reaction in aqueous solution. *Am J Nucl Med Mol Imaging.* 2014;4:303–310.
16. Chen Y, Pullambhatla M, Foss CA, et al. 2-(3-{1-carboxy-5-[(6-[^{18}F]fluoro-pyridine-3-carbonyl)-amino]-pentyl}-ureido)-pentanedioic acid, [^{18}F]DCFPyL, a PSMA-based PET imaging agent for prostate cancer. *Clin Cancer Res.* 2011; 17:7645–7653.
17. Giesel FL, Cardinale J, Schäfer M, et al. ^{18}F-labelled PSMA-1007 shows similarity in structure, biodistribution and tumour uptake to the theragnostic compound PSMA-617. *Eur J Nucl Med Mol Imaging.* 2016;43:1929–1930.
18. Olberg DE, Arukwe JM, Grace D, et al. One step radiosynthesis of 6-[^{18}F] fluoronicotinic acid 2,3,5,6-tetrafluorophenyl ester ([^{18}F]F-Py-TFP): a new prosthetic group for efficient labeling of biomolecules with fluorine-18. *J Med Chem.* 2010;53:1732–1740.
19. Schäfer M, Bauder-Wüst U, Leotta K, et al. A dimerized urea-based inhibitor of the prostate-specific membrane antigen for ^{68}Ga-PET imaging of prostate cancer. *EJNMMI Res.* 2012;2:23.
20. Bacich DJ, Pinto JT, Tong WP, Heston WDW. Cloning, expression, genomic localization, and enzymatic activities of the mouse homolog of prostate-specific membrane antigen/NAALADase/folate hydrolase. *Mamm Genome.* 2001;12:117–123.
21. Liu T, Toriyabe Y, Kazak M, Berkman CE. Pseudoirreversible inhibition of prostate-specific membrane antigen by phosphoramidate peptidomimetics. *Biochemistry.* 2008;47:12658–12660.
22. Barrett JA, Coleman RE, Goldsmith SJ, et al. First-in-man evaluation of 2 high-affinity PSMA-avid small molecules for imaging prostate cancer. *J Nucl Med.* 2013;54:380–387.
23. Zechmann CM, Afshar-Oromieh A, Armor T, et al. Radiation dosimetry and first therapy results with a ^{124}I/^{131}I-labeled small molecule (MIP-1095) targeting PSMA for prostate cancer therapy. *Eur J Nucl Med Mol Imaging.* 2014;41: 1280–1292.
24. Vallabhajosula S, Nikolopoulou A, Babich JW, et al. ^{99m}Tc-labeled small-molecule inhibitors of prostate-specific membrane antigen: pharmacokinetics and biodistribution studies in healthy subjects and patients with metastatic prostate cancer. *J Nucl Med.* 2014;55:1791–1798.
25. Cho SY, Gage KL, Mease RC, et al. Biodistribution, tumor detection, and radiation dosimetry of ^{18}F-DCFBC, a low-molecular-weight inhibitor of prostate-specific membrane antigen, in patients with metastatic prostate cancer. *J Nucl Med.* 2012;53:1883–1891.
26. Rowe SP, Macura KJ, Mena E, et al. PSMA-based [^{18}F]DCFPyL PET/CT is superior to conventional imaging for lesion detection in patients with metastatic prostate cancer. *Mol Imaging Biol.* 2016;18:411–419.
27. Weineisen M, Schottelius M, Simecek J, et al. ^{68}Ga- and ^{177}Lu-labeled PSMA I&T: optimization of a PSMA-targeted theranostic concept and first proof-of-concept human studies. *J Nucl Med.* 2015;56:1169–1176.